

Chapter 3

Determination of the Strong Coupling Constant

The inclusive jet production cross-section at hadron colliders mainly depends on the strong coupling constant α_S for a given centre-of-mass energy. Hence the measurements of the inclusive jet cross-section and jet properties provide a direct probe to measure the strong coupling constant. The measurement of α_S has been already done by various experiments such as CMS [17, 26, 45–47], ATLAS [48], D0 [49, 50], H1 [51, 52], and ZEUS [53]. In this thesis, the measurements of differential inclusive 2-jet and 3-jet event cross-sections as well as the cross-section ratio R_{32} , as a function of $H_{T,2}/2$ are used to extract the value of the strong coupling constant at the scale of the Z boson mass $\alpha_s(M_Z)$. The differential inclusive jet production cross-section upto at NLO is given by [54] :

$$\frac{d\sigma}{d(H_{T,2}/2)} = \alpha_S^2(\mu_r) \hat{X}^{(0)}(\mu_f, H_{T,2}/2) [1 + \alpha_S(\mu_r) K1(\mu_r, \mu_f, H_{T,2}/2)] \quad (3.1)$$

where $\frac{d\sigma}{d(H_{T,2}/2)}$ is the differential inclusive jet production cross-section as a function of $H_{T,2}/2$, μ_r and μ_f are the renormalization and factoriza-

tion scales set equal to $H_{T,2}/2$, $\alpha_S^2(\mu_r)\hat{X}^{(0)}(\mu_f, H_{T,2}/2)$ is the leading order (LO) contribution to the differential inclusive jet production cross-section and $\alpha_S^3(\mu_r)\hat{X}^{(0)}(\mu_f, H_{T,2}/2)K1(\mu_r, \mu_f, H_{T,2}/2)$ is the next-to-leading order (NLO) contribution. Equation 3.1 shows how the inclusive jet production cross-section varies with $\alpha_s(\mu_r)$.

3.1 Sensitivity of Measurements to $\alpha_s(M_Z)$

For a fixed choice of μ_r and μ_f , different input values of $\alpha_s(M_Z)$ to a PDF set will lead to different theory predictions of the differential cross-section distribution. This will give an estimate of the sensitivity of the theory predictions to the varying input value of $\alpha_s(M_Z)$. A comparison of the measured spectrum with the theory predictions obtained using all $\alpha_s(M_Z)$ inputs will give a hint of the input value of $\alpha_s(M_Z)$ for which the theory distribution has the closest matching with data. In this section, the sensitivity of the inclusive differential jet event cross-sections and cross-section ratio, R_{32} to varying input values of $\alpha_s(M_Z)$ for different PDF sets is demonstrated by plotting the ratios of data over theory predictions with central value of $\alpha_s(M_Z)$.

Figures 3.1, 3.2 and 3.3 present the ratio of data to the theory predictions, corrected for NP effects, for all variations in $\alpha_s(M_Z)$ available for the PDF sets CT10, CT14, MSTW2008, MMHT2014 and NNPDF2.3 at NLO evolution order as specified in Table 2.1, for inclusive 2-jet, inclusive 3-jet events cross-section and ratio R_{32} respectively. The $\alpha_s(M_Z)$ value is varied in the range 0.112-0.127, 0.111-123, 0.110-0.130, 0.108-0.128 and 0.114-0.124 in steps of 0.001 for the CT10, CT14, MSTW2008, MMHT2014 and NNPDF2.3 PDF sets, respectively. The error bars correspond to the total experimental uncertainty derived as quadratic sum from all uncertainty sources. The theory predictions are also corrected for EW effects for inclusive 2-jet events cross-section. A small slope increasing with $H_{T,2}/2$ is visible

for most PDFs in both cross-sections. This effect is largely cancelled in the cross-section ratio. R_{32} exhibits a flat behaviour with respect to the predictions for all five PDF sets in the whole range of $H_{T,2}/2$ up to 1680 GeV. Therefore, these data [3] can be used to determine the strong coupling constant, although only up to 1 TeV for the cross-sections as long as electroweak corrections are not taken into account.

Moreover, the different sensitivity to $\alpha_s(M_Z)$ caused by the leading power in α_S in the expansion of the 2-jet inclusive ($\propto \alpha_S^2$) and the 3-jet inclusive cross-section ($\propto \alpha_S^3$), and their ratio ($\propto \alpha_S^1$) is clearly visible from the spread between the calculations for the smallest and largest value of $\alpha_s(M_Z)$ within the same PDF set when passing through Figures 3.1–3.3. This also demonstrates the potential of ratios R_{mn} with $m-n > 1$.

3.2 Determination of $\alpha_s(M_Z)$

As discussed in the previous section, the measured inclusive 2-jet and 3-jet event cross-sections [6] and their ratio [12] R_{32} can be used for a determination of the strong coupling constant $\alpha_s(M_Z)$. To extract the value of $\alpha_s(M_Z)$, a general fit procedure [17] [45, 47] has been followed and is described in the following section.

3.2.1 Fitting Procedure

The value of $\alpha_s(M_Z)$ is determined by minimizing the chi-square (χ^2) [1] between the experimental measurement and the theoretical predictions. The χ^2 is defined as:

$$\chi^2 = M^T C^{-1} M \quad (3.2)$$

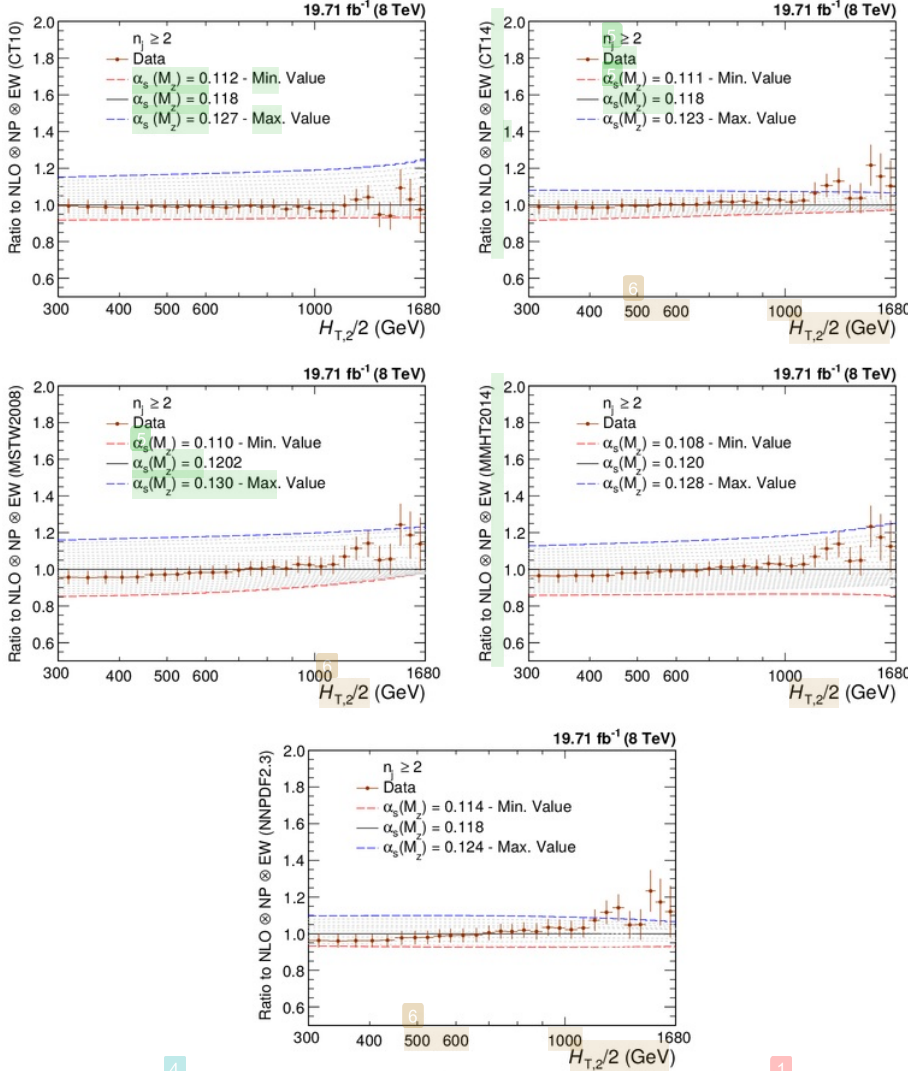


Figure 3.1: Ratio of the inclusive 2-jet differential cross-section to theory predictions using the CT10 (top left), the CT14 (top right), the MSTW2008 (middle left), the MMHT2014 (middle right) and NNPDF2.3 (bottom) NLO PDF sets for a series of values of $\alpha_s(M_Z)$. The $\alpha_s(M_Z)$ value is varied in the range 0.112-0.127, 0.111-0.123, 0.110-0.130, 0.108-0.128 and 0.114-0.124 in steps of 0.001 for the CT10, CT14, MSTW2008, MMHT2014 and NNPDF2.3 NLO PDF sets, respectively. The error bars correspond to the total experimental uncertainty. The theory predictions are corrected for non-perturbative (NP) and electroweak (EW) effects.

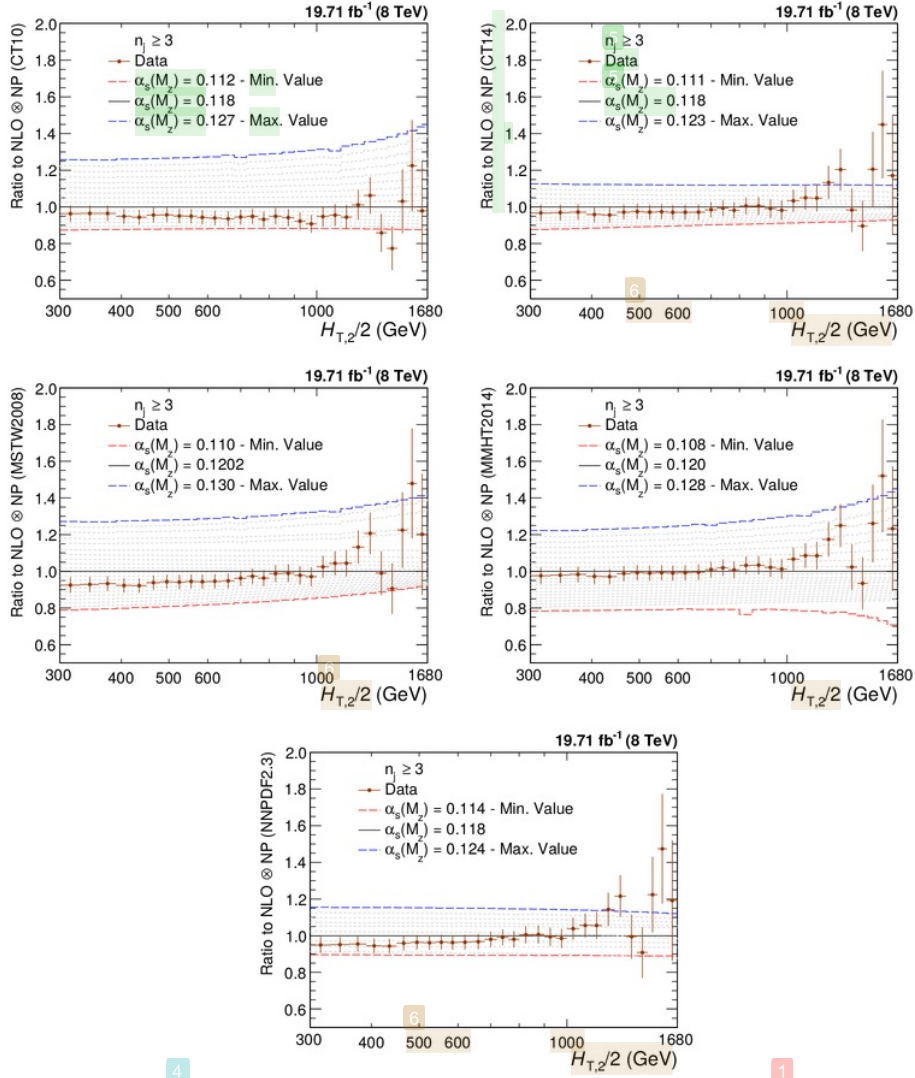


Figure 3.2: Ratio of the inclusive 3-jet differential cross-section to theory predictions using the CT10 (top left), the CT14 (top right), the MSTW2008 (middle left), the MMHT2014 (middle right) and NNPDF2.3 (bottom) NLO PDF sets for a series of values of $\alpha_s(M_Z)$. The $\alpha_s(M_Z)$ value is varied in the range 0.112-0.127, 0.111-1.23, 0.110-0.130, 0.108-0.128 and 0.114-0.124 in steps of 0.001 for the CT10, CT14, MSTW2008, MMHT2014 and NNPDF2.3 NLO PDF sets, respectively. The error bars correspond to the total experimental uncertainty. The theory predictions are corrected for non-perturbative (NP) effects.

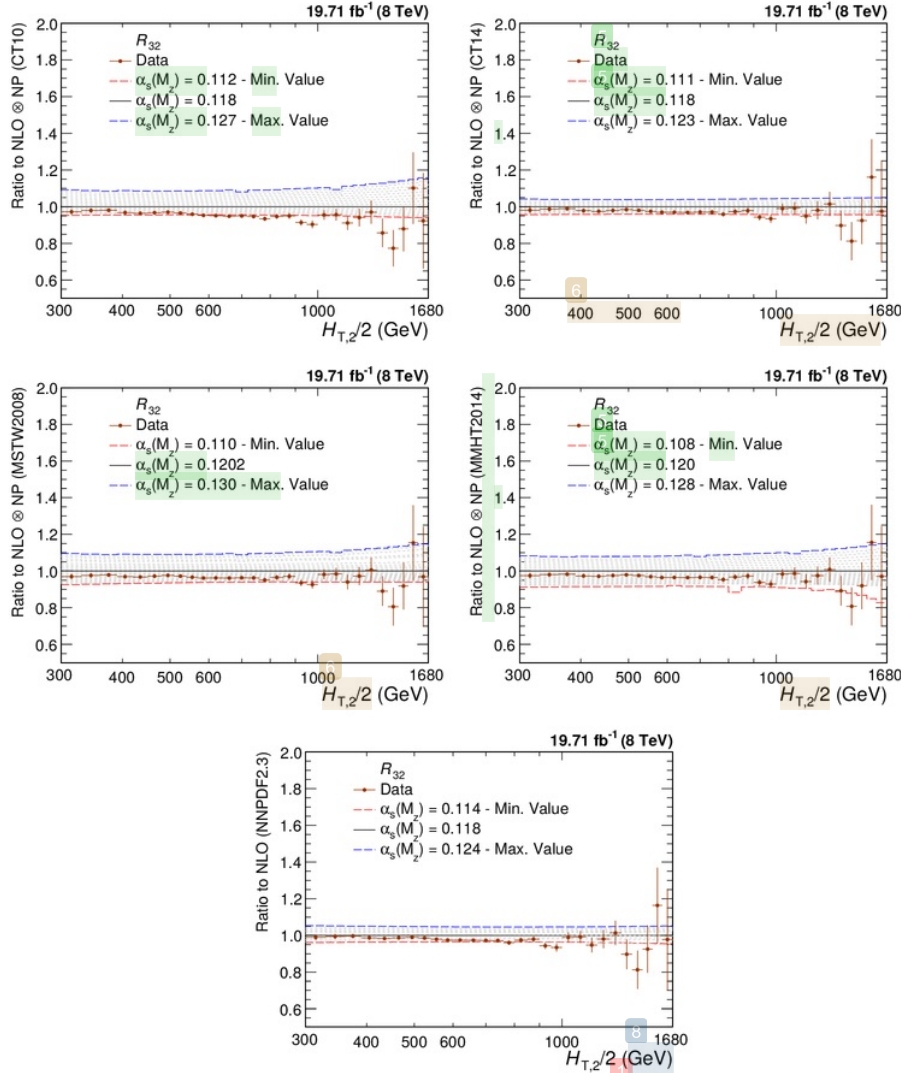


Figure 3.3: Ratio of the cross-section ratio, R_{32} to theory predictions using the CT10 (top left), the CT14 (top right), the MSTW2008 (middle left), the MMHT2014 (middle right) and NNPDF2.3 (bottom) NLO PDF sets for a series of values of $\alpha_s(M_Z)$. The $\alpha_s(M_Z)$ value is varied in the range 0.112-0.127, 0.111-123, 0.110-0.130, 0.108-0.128 and 0.114-0.124 in steps of 0.001 for the CT10, CT14, MSTW2008, MMHT2014 and NNPDF2.3 NLO PDF sets, respectively. The error bars correspond to the total experimental uncertainty. The theory predictions are corrected for non-perturbative (NP) effects.

¹ where M is the vector of the differences between the data (D^i) and the theoretical values (T^i) in each bin i ,

$$M^i = D^i - T^i \quad (3.3)$$

³ and C is the covariance matrix including all experimental uncertainties as described in Sec. 1.6 and some theoretical uncertainties discussed in Sec. 2.2. The covariance matrix $C = C_{\text{exp}} + C_{\text{theo}}$ is defined as the sum of covariances of experimental and theoretical sources of uncertainty as follows :

$$C_{\text{exp}} = \text{Cov}^{\text{ExpStat}} + \sum \text{Cov}^{\text{JEC}} + \text{Cov}^{\text{Unfolding}} + \text{Cov}^{\text{Lumi}} + \text{Cov}^{\text{Residual}} \quad (3.4)$$

$$C_{\text{theo}} = \text{Cov}^{\text{TheoStat}} + \text{Cov}^{\text{NP}} + \text{Cov}^{\text{PDF}} \quad (3.5)$$

where the labelled covariance matrices account for the following effects:

- $\text{Cov}^{\text{ExpStat}}$: statistical uncertainty of the data including correlations introduced by the unfolding
- Cov^{JEC} : the jet energy corrections (JEC) systematic uncertainty
- $\text{Cov}^{\text{Unfolding}}$: the unfolding systematic uncertainty including the resolution (JER) and model dependence
- Cov^{Lumi} : the luminosity uncertainty
- $\text{Cov}^{\text{Residual}}$: a residual uncorrelated systematic uncertainty summarizing individual causes such as small trigger and identification inefficiencies, time dependence of the jet p_T resolution, and uncertainty on the trigger prescale factors
- $\text{Cov}^{\text{TheoStat}}$: statistical uncertainty caused by numerical integrations in the cross-section computations

- Cov^{NP} : the systematic uncertainty of the non-perturbative (NP) corrections
- Cov^{PDF} : the PDF uncertainties

While taking the differences between theory and data, the treatment of experimental and theoretical systematic uncertainties is crucial. The Unfolding, JEC, Lumi and PDF and NP systematic uncertainties are treated as 100% correlated among $H_{\text{T},2}/2$ bins. If δ_i is the total uncertainty on the differential cross-section, for the i -th $H_{\text{T},2}/2$ bin, for any of these fully correlated sources, then the i,j -th element of the corresponding covariance matrix is given by $\text{COV}_{ij} = \delta_i \times \delta_j$. The JEC, unfolding, and luminosity uncertainties are treated as multiplicative to avoid the statistical bias that arises when estimating uncertainties from data. In fits of the ratio R_{32} , the luminosity and residual uncorrelated uncertainties cancel completely. Partial cancellations between the other sources of uncertainty are taken into account in the fit.

The evaluation of PDF uncertainty depends on the individual PDF set as already discussed in Sec. 2.2.2. The PDF covariance matrix construction varies among different PDF sets. The CT10, CT14, MMHT2014 and MSTW2008 NLO PDF sets employ the eigenvector method to evaluate the PDF uncertainties as explained in Sec. 2.2.2. The number of eigenvectors (N_{ev}) with two PDF members per eigenvector for CT10, CT14, MMHT2014 and MSTW2008 NLO PDF sets are 26, 28, 25 and 20, respectively. The NNPDF2.3 PDF set comes with hundred different replicas (N_{rep}) instead of different eigenvectors, as for CT10 or CT14 PDF sets. The mean uncertainty is calculated as average uncertainty from 100 different replicas. Following the prescription given in [55], the PDF uncertainty is calculated as :

$$(\Delta X)^2 = \frac{1}{N_{\text{rep}} - 1} \sum_{k=1}^{N_{\text{rep}}} [X_k - \langle X_k \rangle]^2 \quad (3.6)$$

where ΔX is the uncertainty on predicted differential cross-section, X_k is the

differential cross-section for k -th replica and $\langle X_k \rangle$ is the average differential cross-section from all the replicas.

Scale uncertainties of the pQCD predictions are taken into account by employing the offset method, i.e. by performing separate fits with varying scale factors as described in the Sec. 2.2.1. The largest upwards and downwards deviations from the default factors are defined as the uncertainty. At NLO such scale variations predominantly lead to smaller cross-sections and also a smaller ratio R_{32} as visible in Fig. 2.5. As a consequence the scale uncertainty in fits is equally asymmetric, where smaller cross-sections or ratios are compensated by an increase in the fitted value for $\alpha_s(M_Z)$.

3.2.2 Fit Results

To determine the value of the strong coupling constant at the scale of the Z boson mass $\alpha_s(M_Z)$, fits to the differential inclusive 2-jet and 3-jet events cross-sections are performed using five different NLO PDF sets : CT10, CT14, MSTW2008, MMHT2014 and NNPDF2.3. The range in $H_{T,2}/2$ is restricted to be between 300 GeV and 1 TeV to avoid the region close to the minimal p_T threshold of 150 GeV for each jet at low p_T and the onset of electroweak effects at high $H_{T,2}/2$, which are available for the dijet case only. The $\alpha_s(M_Z)$ results obtained from a simultaneous fit to all 19 $H_{T,2}/2$ bins in the above mentioned range are reported in Table 3.1. For comparison, a simultaneous fit to both cross-sections ignoring any correlations, and a fit to the cross-section ratio R_{32} , fully accounting for correlations is also performed and the results are tabulated in Table 3.2. The electroweak effects are assumed to cancel in the ratio as do the luminosity and the uncorrelated uncertainty.

All cross-section fits give compatible values for $\alpha_s(M_Z)$ in the range of 0.115-0.118 whereas for the ratio R_{32} somewhat smaller values are obtained. But for individual cross-sections, χ^2/n_{dof} values are small as compared to the cross-section

ratio R_{32} . A possible explanation is an overestimation of the residual uncorrelated uncertainty of 1% that is cancelled for R_{32} . If the fits are repeated with an assumed uncertainty of 0.25% instead, the χ^2/n_{dof} values lie around unity while the $\alpha_s(M_Z)$ values are still compatible with the previous results but with slightly reduced uncertainties.

Table 3.1: Determination of $\alpha_s(M_Z)$ from the inclusive 2-jet and 3-jet event cross-sections using five PDF sets at NLO. Only total uncertainties without scale variations are quoted. The results are obtained from a simultaneous fit to all 19 $H_{\text{T},2}/2$ bins in the restricted range of $0.3 < H_{\text{T},2}/2 < 1.0 \text{TeV}$.

PDF set	Inclusive 2-jets			Inclusive 3-jets		
	$\alpha_s(M_Z)$	$\pm \Delta \alpha_s(M_Z)$	χ^2/n_{dof}	$\alpha_s(M_Z)$	$\pm \Delta \alpha_s(M_Z)$	χ^2/n_{dof}
CT10	0.1174	0.0032	3.0/18	0.1169	0.0027	5.4/18
CT14	0.1160	0.0035	3.5/18	0.1159	0.0031	6.1/18
MSTW2008	0.1159	0.0025	5.3/18	0.1161	0.0021	6.7/18
MMHT2014	0.1165	0.0034	5.9/18	0.1166	0.0025	7.1/18
NNPDF2.3	0.1183	0.0025	9.7/18	0.1179	0.0021	9.1/18

Table 3.2: Determination of $\alpha_s(M_Z)$ from the inclusive 2-jet and 3-jet event cross-sections simultaneously and from their ratio R_{32} using five PDF sets at NLO. Only total uncertainties without scale variations are quoted. The results are obtained from a simultaneous fit to all 38 (left) and 19 (right) $H_{\text{T},2}/2$ bins in the restricted range of $0.3 < H_{\text{T},2}/2 < 1.0 \text{ TeV}$. For comparison, correlations between the two cross-sections are neglected in the simultaneous fit on the left, but fully taken into account in the ratio fit on the right.

PDF set	Inclusive 2- and 3-jets			R_{32}		
	$\alpha_s(M_Z)$	$\pm \Delta \alpha_s(M_Z)$	χ^2/n_{dof}	$\alpha_s(M_Z)$	$\pm \Delta \alpha_s(M_Z)$	χ^2/n_{dof}
CT10	0.1170	0.0026	8.2/37	0.1141	0.0028	19./18
CT14	0.1161	0.0029	9.1/37	0.1139	0.0032	15./18
MSTW2008	0.1161	0.0021	11./37	0.1150	0.0023	21./18
MMHT2014	0.1168	0.0025	11./37	0.1142	0.0022	19./18
NNPDF2.3	0.1188	0.0019	15./37	0.1184	0.0021	12./18

To investigate how the electroweak (EW) corrections affect the fit results for $\alpha_s(M_Z)$, the range in $H_{\text{T},2}/2$ is extended to $0.3 < H_{\text{T},2}/2 < 1.68 \text{ TeV}$. $\alpha_s(M_Z)$ values are obtained from fits to the inclusive 2-jet event cross-section in this range with or without EW correction factors and the results are presented in Table 3.3. The largest impact is a reduction in χ^2/n_{dof} , which indicates a better agreement when

EW effects are included. In addition, a tendency to slightly smaller $\alpha_s(M_Z)$ values is observed without the EW corrections. For the ratio R_{32} , it is expected that these effects are much reduced.

²
Table 3.3: Determination of $\alpha_s(M_Z)$ from the inclusive 2-jet event cross-section using five PDF sets at NLO without (left) and with (right) electroweak (EW) corrections. Only total uncertainties without scale variations are quoted. The results are obtained from a simultaneous fit to all 29 $H_{T,2}/2$ bins in the range of $0.3 < H_{T,2}/2 < 1.68$ TeV.

PDF set	without EW			with EW		
	$\alpha_s(M_Z)$	$\pm\Delta\alpha_s(M_Z)$	χ^2/n_{dof}	$\alpha_s(M_Z)$	$\pm\Delta\alpha_s(M_Z)$	χ^2/n_{dof}
CT10	0.1163	0.0034	15./28	0.1165	0.0032	14./28
CT14	0.1137	0.0033	24./28	0.1144	0.0033	17./28
MSTW2008	0.1093	0.0028	27./28	0.1133	0.0023	19./28
MMHT2014	0.1127	0.0032	32./28	0.1141	0.0032	21./28
NNPDF2.3	0.1162	0.0024	31./28	0.1168	0.0024	23./28

From Fig. 3.3 follows that only the PDF sets MSTW2008 and MMHT2014 provide a large enough range in $\alpha_s(M_Z)$ values to ensure fits without extrapolation. The other three PDF sets are at the limit such that reliable fits cannot be performed for all scale settings and/or bins in scale $Q = H_{T,2}/2$. Since many systematic uncertainties cancel completely or partially in the cross-section ratio R_{32} as compared to the individual cross-sections, R_{32} is used mainly to determine the value of $\alpha_s(M_Z)$. Table 3.4 give the complete results for MSTW2008 and MMHT2014 for the full range in $H_{T,2}/2$ of 300 GeV up to 1.68 TeV along with the corresponding components of PDF, scale, NP and total experimental except scale uncertainties are shown.
¹
In contrast to fits at NLO using cross-sections where the scale uncertainty recipe usually leads to a very asymmetric behaviour with larger downward uncertainties in the case, this is inverted for the fits to the cross-section ratio R_{32} . The scale uncertainty is the most dominant source of total uncertainty on $\alpha_s(M_Z)$. These values are determined with the central renormalization and factorization scales i.e. $\mu_r = \mu_f = H_{T,2}/2$. The values are also determined for the six scale factor combinations for the two PDF sets MSTW2008 and MMHT2014 and results are shown in Table 3.5.

The uncertainty composition for $\alpha_s(M_Z)$ determined from cross section ratio R_{32} is performed in four sub-ranges of $H_{T,2}/2$ and the results are shown in Table 3.6. The statistical uncertainty of the NLO computation is negligible in comparison to any of the other sources of uncertainty. Electroweak corrections, significant only at high $H_{T,2}/2$, are assumed to cancel between the numerator and denominator.

Using the MSTW2008 PDF set, which dates from before the LHC start, the strong coupling constant finally is determined to

$$\begin{aligned} \alpha_s(M_Z) &= 0.1150 \pm 0.0010 \text{ (exp)} \pm 0.0013 \text{ (PDF)} \pm 0.0015 \text{ (NP)} {}^{+0.0050}_{-0.0000} \text{ (scale)} \\ &= 0.1150 \pm 0.0023 \text{ (all except scale)} {}^{+0.0050}_{-0.0000} \text{ (scale)} \end{aligned} \quad (3.7)$$

The MMHT2014 PDF set, although using LHC jet data to determine the PDF parameters, leads to a very similar result of

$$\begin{aligned} \alpha_s(M_Z) &= 0.1142 \pm 0.0010 \text{ (exp)} \pm 0.0013 \text{ (PDF)} \pm 0.0014 \text{ (NP)} {}^{+0.0049}_{-0.0006} \text{ (scale)} \\ &= 0.1142 \pm 0.0022 \text{ (all except scale)} {}^{+0.0049}_{-0.0006} \text{ (scale)} \end{aligned} \quad (3.8)$$

3.3 ² Running of the Strong Coupling Constant

The value of the strong coupling constant α_S ¹⁴ depends on the energy scale Q and it decreases with the increase of scale Q . To study this dependence, the determination of α_S is carried out at different energies. The procedure to extract $\alpha_S(Q)$ is same as the one followed for the $\alpha_s(M_Z)$. To have different energy scales, the fitted $H_{T,2}/2$ range 300 - 1680 GeV is divided into four different sub-ranges as shown by the first column in Table 3.7. Each of the $H_{T,2}/2$ range is associated with a scale Q , which

Table 3.4: Determination of $\alpha_s(M_Z)$ from the ratio R_{32} using the two most compatible PDF sets MSTW2008 and MMHT2014 at NLO along with the corresponding components of PDF, scale, NP and total (except scale) experimental uncertainties. The results are obtained from a simultaneous fit to all 29 $H_{T,2}/2$ bins in the full range of $0.3 < H_{T,2}/2 < 1.68$ TeV.

PDF set	$R_{32}: \Delta\alpha_s(M_Z) \times 1000$						
	$\alpha_s(M_Z)$	exp	PDF	NP	all exc.	scale	χ^2/n_{dof}
MSTW2008	0.1150	± 10	± 13	± 15	± 23	$^{+50}_{-0}$	26./28
MMHT2014	0.1142	± 10	± 13	± 14	± 22	$^{+49}_{-6}$	24./28

Table 3.5: Determination of $\alpha_s(M_Z)$ from the ratio R_{32} in the $H_{T,2}/2$ range from 0.3 up to 1.68 TeV at the central scale and for the six scale factor combinations for the two PDF sets MSTW2008 and MMHT2014.

$\mu_r/H_{T,2}/2$	$\mu_f/H_{T,2}/2$	MSTW2008		MMHT2014	
		$\alpha_s(M_Z)$	χ^2/n_{dof}	$\alpha_s(M_Z)$	χ^2/n_{dof}
1	1	0.1150	26./28	0.1142	24./28
1/2	1/2	0.1165	77./28	0.1160	73./28
2	2	0.1200	18./28	0.1191	18./28
1/2	1	0.1150	53./28	0.1136	48./28
1	1/2	0.1150	30./28	0.1142	28./28
1	2	0.1155	23./28	0.1147	22./28
2	1	0.1180	19./28	0.1175	19./28

Table 3.6: Uncertainty composition for $\alpha_s(M_Z)$ from the determination of α_S from the jet event rate R_{32} in bins of $H_{T,2}/2$. The statistical uncertainty of the NLO computation is negligible in comparison to any of the other sources of uncertainty. Electroweak corrections, significant only at high $H_{T,2}/2$, are assumed to cancel between the numerator and denominator.

$H_{T,2}/2$ (GeV)	MSTW2008: $\Delta\alpha_s(M_Z) \times 1000$					MMHT2014: $\Delta\alpha_s(M_Z) \times 1000$				
	$\alpha_s(M_Z)$	exp	PDF	NP	scale	$\alpha_s(M_Z)$	exp	PDF	NP	scale
300–420	0.1157	± 15	± 14	± 19	$^{+53}_{-0}$	0.1158	± 14	± 10	± 19	$^{+52}_{-0}$
420–600	0.1153	± 11	± 14	± 18	$^{+57}_{-0}$	0.1154	± 11	± 12	± 17	$^{+56}_{-0}$
600–1000	0.1134	± 13	± 16	± 19	$^{+52}_{-0}$	0.1140	± 12	± 12	± 18	$^{+45}_{-0}$
1000–1680	0.1147	± 29	± 17	± 18	$^{+63}_{-11}$	0.1154	± 25	± 14	± 15	$^{+56}_{-11}$
300–1680	0.1150	± 10	± 13	± 15	$^{+50}_{-0}$	0.1142	± 10	± 13	± 14	$^{+49}_{-6}$

is the differential cross section weighted average $H_{T,2}/2$ scale from the inclusive 2-jet calculations and integrated over all the measured $H_{T,2}/2$ bins contributing to that given $H_{T,2}/2$ range. Let N_{bin}^j be the total number of measured $H_{T,2}/2$ bins contributing to the j -th $H_{T,2}/2$ range, then the corresponding scale Q_j , shown in second column of Table 3.7, is calculated as :

$$Q_j = \frac{\sum_{i=1}^{N_{bin}^j} H_{T,2}^i \left[\frac{d\sigma}{d(H_{T,2}/2)} \right]^i}{\sum_{i=1}^{N_{bin}^j} \left[\frac{d\sigma}{d(H_{T,2}/2)} \right]^i} \quad (3.9)$$

The value of $\alpha_s(M_Z)$ is extracted in each $H_{T,2}/2$ range. These extracted $\alpha_s(M_Z)$ values are evolved to the corresponding values $\alpha_S(Q)$ and are quoted in Table 3.7 along with the extracted $\alpha_s(M_Z)$ values and the total uncertainty. The evolution is performed for five flavours at 2-loop order with the RUNDEC program [56, 57]. The obtained $\alpha_S(Q)$ points (black solid circles) are shown as a function of scale Q in Fig. 3.4. The black solid line and the yellow uncertainty band are evolved using $\alpha_s(M_Z) = 0.1150 \pm 0.0023$ (all except scale) $^{+0.0050}_{-0.0000}$ (scale) obtained using MSTW2008 NLO PDF set. The world average [58] (dashed line) and results from other measurements of the CMS [17, 26, 45–47], ATLAS [48], D0 [49, 50], H1 [51, 52], and ZEUS [53] experiments are also imposed. The current measurement is in very good agreement within the uncertainty with other results obtained by previous experiments as well as with the world average value of $\alpha_s(M_Z) = 0.1181 \pm 0.0011$ derived in Ref. [58].

Table 3.7: Evolution of the strong coupling constant between the scale of the Z boson mass and the cross-section averaged $H_{T,2}/2$ scale $\langle Q \rangle$ for the separate determinations in each respective fit range. The evolution is performed for five flavours at 2-loop order with the RUNDEC program [56, 57].

$H_{T,2}/2$ (GeV)	$\langle Q \rangle$ (GeV)	$\alpha_s(M_Z)$	$\alpha_s(Q)$	No. of data points	χ^2/n_{dof}
300-420	340	$0.1157^{+0.0060}_{-0.0030}$	$0.0969^{+0.0041}_{-0.0021}$	4	2.8/3
420-600	476	$0.1153^{+0.0062}_{-0.0025}$	$0.0928^{+0.0039}_{-0.0016}$	6	6.1/5
600-1000	685	$0.1134^{+0.0059}_{-0.0028}$	$0.0879^{+0.0035}_{-0.0017}$	9	7.1/8
1000-1680	1114	$0.1147^{+0.0074}_{-0.0040}$	$0.0841^{+0.0039}_{-0.0021}$	10	5.4/9

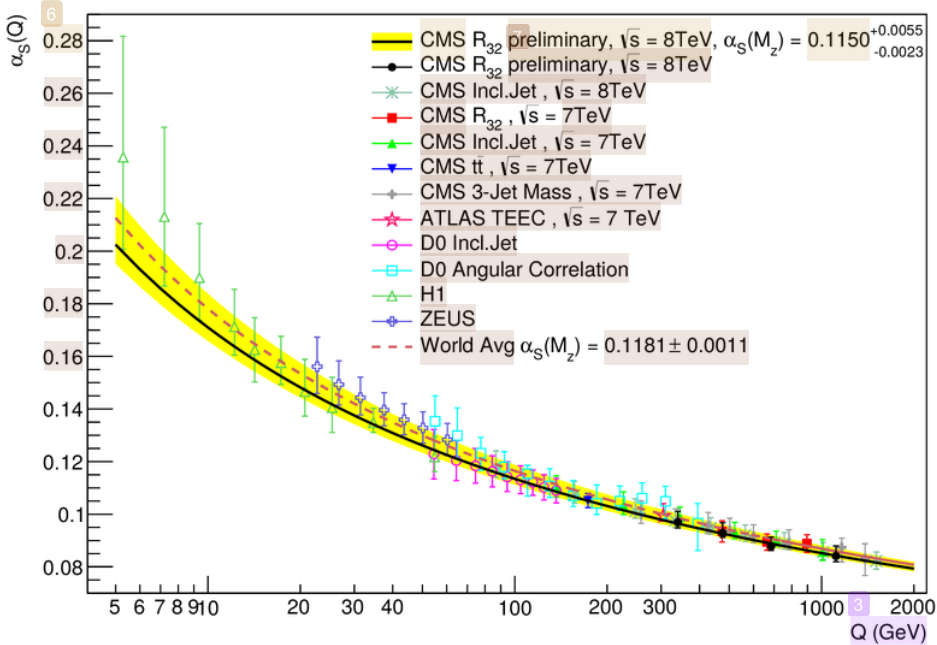


Figure 3.4: The running $\alpha_s(Q)$ as a function of the scale Q is shown as obtained by using the MSTW2008 NLO PDF set. The solid line and the uncertainty band are drawn by evolving the extracted $\alpha_s(M_Z)$ values using the 2-loop 5-flavour renormalization group equations as implemented in RUNDEC [56, 57]. The dashed line represents the evolution of the world average [58] and the black circles correspond to the $\alpha_s(Q)$ determinations presented in Table 3.7. Results from other measurements of CMS [17, 26, 45–47], ATLAS [48], D0 [49, 50], H1 [51, 52], and ZEUS [53] are superimposed.